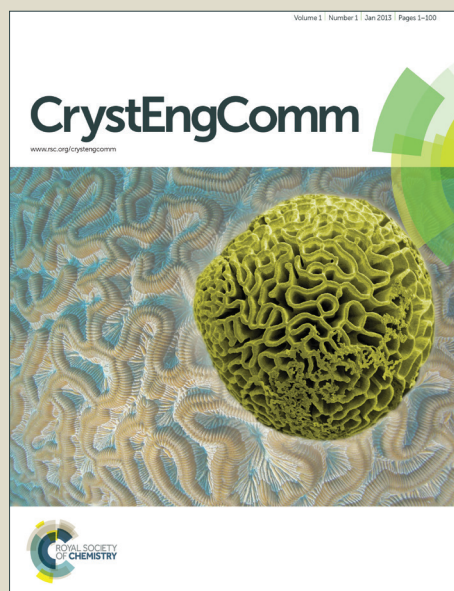


CrystEngComm

Accepted Manuscript



This is an *Accepted Manuscript*, which has been through the Royal Society of Chemistry peer review process and has been accepted for publication.

Accepted Manuscripts are published online shortly after acceptance, before technical editing, formatting and proof reading. Using this free service, authors can make their results available to the community, in citable form, before we publish the edited article. We will replace this *Accepted Manuscript* with the edited and formatted *Advance Article* as soon as it is available.

You can find more information about *Accepted Manuscripts* in the [Information for Authors](#).

Please note that technical editing may introduce minor changes to the text and/or graphics, which may alter content. The journal's standard [Terms & Conditions](#) and the [Ethical guidelines](#) still apply. In no event shall the Royal Society of Chemistry be held responsible for any errors or omissions in this *Accepted Manuscript* or any consequences arising from the use of any information it contains.

Growth, structure, luminescence and mechanical resonance of Bi₂O₃ nano- and microwires

María Vila^a, Carlos Díaz - Guerra^a, Javier Piqueras^a, Lluís López - Conesa^b, Sònia Estradé^{b,c},
Francesca Peiró^b

^a *Departamento de Física de Materiales, Facultad de Ciencias Físicas, Universidad Complutense de Madrid, 28040 Madrid, Spain.*

^b *LENS, MIND-IN2UB, Departament d'Electrònica, Universitat de Barcelona, Martí i Franquès 1, 08028 Barcelona, Spain.*

^c *TEM-MAT, CCiT, Universitat de Barcelona, Solé i Sabarís 1, 08028 Barcelona, Spain*

Abstract

α -Bi₂O₃ hierarchical structures formed by multi-branched micro- and nanowires have been grown by an evaporation-deposition method. The morphology, composition, structure, as well as several physical properties of the obtained nanowires have been investigated. The relative intensities of photoluminescence bands related to Bi²⁺ ions and oxygen vacancies have been found to depend on the composition of the precursor used in the growth process. In-situ scanning electron microscope measurements of the mechanical resonance frequency of the microwires have been used to determine their Young's modulus, which was found to depend on the wire dimensions, with values ranging from 11 GPa to 284 GPa. The quality factors measured suggest that Bi₂O₃ wires may have potential applications as micromechanical resonators.

1. Introduction

Semiconductor nanowires are considered as essential building blocks for the development of future electronic and optical nanodevices.¹⁻³ In particular, the growth and physical properties of nanowires of certain binary oxides - such as ZnO, In₂O₃ or SnO₂ - have been often reported,⁴⁻⁶ while elongated nanostructures of other oxides of technological interest have been investigated to a much lesser extent. This is the case of Bi₂O₃, a wide band gap semiconductor with reported E_g values ranging between 2.85 eV and 3.25 eV,^{7,8} which shows a good photoconductive behaviour, a high ionic conductivity and refraction index and can be also used as a host of optically active ions.⁹⁻¹² Bi₂O₃ has four main crystallographic polymorphs. The monoclinic α phase and the face centred cubic δ phase are stable at room and high temperature, respectively. Two metastable phases, the tetragonal β phase and the body centred cubic γ phase, result from the cooling of the high temperature δ phase. Mixed phase (α and β) Bi₂O₃ nanowires have been synthesized by a thermal oxidation method,¹³ while β phase nanowires and nanorods have been grown by chemical vapour deposition¹⁴⁻¹⁶ and thermal evaporation of Bi.¹⁷ The reported α -phase elongated structures include nanowires obtained by chemical routes¹⁸ as well as nano- and microribbons¹⁹ and microrods⁸ grown by vapour deposition methods.

Hierarchical growth leading to the formation of branched structures and, in a more advanced step, to the formation of larger functional units as nanowire networks, is a subject of interest related to the “bottom up” fabrication of nanomaterials.^{20,21} The formation of branched nanostructures and networks, self assembled during evaporation-deposition processes, has been reported for a number of oxide semiconductors. It has been found that the addition of certain metallic elements such as In, Sn or Al, favours the growth of the mentioned complex arrangements.²²⁻²⁷ Thermal growth of hierarchical or, in general, complex branched nanostructures, has been reported for ZnO when small amounts of In₂O₃,²²

SnO_2 ,^{23,24} Eu_2O_3 ²⁵ or Al_2O_3 ²⁶ were added to the precursor material. Morphological changes have been also reported by the addition of SnO_2 in the precursor used to grow GeO_2 ²⁷ or Ga_2O_3 ²⁸ nanowires. The hierarchical growth reported in ref. 22 has been proposed to be related to surface segregation of Sn and this model appears to agree with the side branching observed in refs. 23 and 24. In this work, tin or erbium oxides have been incorporated into a Bi precursor powder to grow, by a vapour-solid method, Bi_2O_3 hierarchical nanostructures formed by rods and nanowires.

Reports on the physical properties of nanowires and other low dimensional structures of Bi_2O_3 are scarce. For this reason, in addition to the morphological, structural and compositional characterization of the grown nanowires - that were carried out by scanning electron microscopy (SEM), high resolution transmission electron microscopy (HRTEM), X-ray diffraction (XRD), electron backscattered diffraction (EBSD) in the SEM and energy-dispersive X-ray microanalysis (EDX) both in the SEM and TEM - their luminescence properties and some aspects of their mechanical behaviour have been investigated. Luminescence was studied by photoluminescence (PL) in a confocal microscope, while the Young's modulus was determined by in-situ SEM measurements of mechanical resonances under an applied electric field. The investigation of mechanical properties on the micro and nanoscale is an important topic for the development and reliability improvement of nano and microelectromechanical systems (MEMS / NEMS) and other devices.

2. Experimental

The precursors used to grow the nanowires were mixtures of Bi powder (Goodfellow 99.997 %) with either SnO_2 (Sigma-Aldrich 99.9 %) or Er_2O_3 (Strem 99.9 %) powders. Mixtures containing Bi and 2, 5 10, 20 or 30 wt. % of SnO_2 were compacted to form disk shaped samples of about 7 mm diameter and 1 mm thickness. Five different mixtures containing 2, 5 10, 20 or 30 wt. % of Er_2O_3 were prepared following the same method. The

samples were then annealed in a horizontal tube furnace, not sealed for vacuum conditions, under argon flow at 800 °C for times between 4 and 10 hours. Transport and oxidation of bismuth took place during the thermal treatments leading to the growth of bismuth oxide nanostructures, nanowires and complex nanowire hierarchical arrangements, on the wall tube. The structures were detached from the tube and deposited on a silicon substrate for characterization. Their morphology and size were investigated with a Fei Inspect SEM. The structure of the wires was investigated by XRD with an X'Pert PRO MRD diffractometer using Cu K α radiation and by HRTEM with a Jeol JEM 2010F and a Jeol JEM 3100F microscope. EBSD of single microwires was performed in a Fei Inspect SEM with a Bruker e-FlashHR⁺ system using an accelerating voltage of 20 kV. The composition of the samples was assessed by EDX in the SEM and TEM by using a Bruker QUANTAX and an Oxford INCA system, respectively. PL measurements were carried out at room temperature in a Horiba Jovin-Ybon LabRAM HR800 system. The samples were excited by a 325 nm He – Cd laser on an Olympus BX 41 confocal microscope. The study of mechanical resonances was carried out on Bi₂O₃ microwires with lengths ranging from 100 to 700 μm and cross sectional dimensions of (0.5 – 3.5) μm . For the synthesis of these larger structures, no Er or Sn oxides were added to the precursor and the growth took place on the compacted Bi₂O₃ disk during annealing at 650 °C for 1.5 h under argon flow. In order to investigate the resonant behaviour of these samples, the disk with the microwires was glued with silver paste on a copper electrode and placed in front of a second copper electrode inside the chamber of a Fei Inspect SEM, as shown in Fig. 1. An oscillating voltage with an amplitude of (3-5) V and a frequency range of (0.1 - 100) kHz was applied with a Stanford Research SR830 DSP lock-in amplifier, while a 20 V constant voltage bias was simultaneously applied with a Keithley 2400 SourceMeter. The amplitude of the oscillating wire was measured, from the SEM images, as function of the voltage frequency and the resonance frequency corresponding to the amplitude

maximum was determined. The Young's modulus of the wire was then calculated from elasticity theory by using the experimental resonance frequencies.

3. Results and discussion

3.1 Morphology, structure and composition

Hierarchical structures formed by a network of branched wires growing from a central axis are observed after the thermal treatment at 800 °C for 10 h of the SnO₂ containing precursor, as shown in the low magnification SEM image of Fig. 2a. These complex architectures were not obtained for shorter treatments. A higher magnification SEM image (Fig. 2b) shows secondary parallel rods with widths of about 1 to 3 μm and smaller perpendicular branches, most of them with cross sectional dimensions of some hundreds of nm. Similar hierarchical structures, as well as wool-like arrangements of thinner wires (100 - 200 nm diameter), are formed when the Er containing precursor is treated also at 800 °C for 10 h (Figs. 2c – 2e). Mixtures with oxide contents (either SnO₂ or Er₂O₃) below 20 wt.% give rise to a lower amount of hierarchical structures, while no noticeable difference, in terms of morphology or density of branched structures, was observed when a mixture containing a 30 wt% of the corresponding oxide was used. In addition, when a mesh of pure Bi was used as the only precursor, just large microrods and microcrystals, without any hierarchical structures, were obtained.⁸ This shows that for Bi₂O₃, as in the case of refs. 21-27, the addition of an atomic fraction of certain cations to the precursor favours the hierarchical growth of oxide nanostructures. It is to be noticed that, contrary to the well known catalyst-assisted vapour-liquid-solid (VLS) nanowire growth, no catalyst nanodrops at the tip of the wires were observed. In fact - as described below - according to the analytical techniques used in the present work, significant amounts of Er and Sn were not incorporated into the as-grown nanostructures. This is probably due to the big difference between our growth temperature

(800 °C) and the melting and boiling temperatures of Er_2O_3 (2345 °C and 3290 °C, respectively) and SnO_2 (1630 °C and 1800 °C, respectively). Although the obtained nanowires do not show a tapered morphology or Bi droplets at their tips, as confirmed by SEM, TEM and EDX measurements, autocatalytic processes cannot be in principle completely discarded. A small thin Bi layer, even atomically flat, might be present at the growth front, which could lead to growth via a VLS mechanism. The layer could be quickly oxidized during cooling or after exposure of the nanostructures to air after the growth, and a subsequent analysis may never find this layer.²⁹ Nevertheless, in the particular case of Bi_2O_3 , the formation of thin Bi layers or droplets has been reported to give rise to samples with micro or nanoribbon morphology.¹⁹ In any case, as previously mentioned, hierarchical Bi_2O_3 arrangements were not obtained after thermal treatments of pure Bi, while a lower density of such arrangements was obtained when mixtures of Bi with low SnO_2 or Er_2O_3 contents were used as precursors. These observations indicate that the addition of both metal oxides play a critical role in the growth of our branched, hierarchical nanostructures, probably increasing the number of nucleation sites, which is related to surface energy of the crystal, temperature, and supersaturated ratio of vapor.³⁰ We believe that growth is governed in the present case by a vapour – solid (VS) process, in which the vapour originates from the precursor in a high temperature zone and thereby facilitates the formation of the micro and nanostructures in a low temperature zone by the assistance of the Ar flow. The VS mechanism has been invoked in order to explain the formation of several hierarchical nanostructures in presence of alloying elements.²²⁻²⁶ The fact that side branching is observed only in the presence of such elements strongly suggests that surface segregation may play an important role. During growth of the central nanowire, the alloying content is continuously segregated to the boundaries of the nanowire core. The alloy rich layer of the boundaries became the nucleation sites for the subsequent growth of side branches.²² As stated before, this mechanism has been proposed to

explain the formation of ZnO hierarchical nanostructures when small amounts of In_2O_3 ,²² SnO_2 ,^{23,24} Eu_2O_3 ²⁵ or Al_2O_3 ²⁶ were added to the precursor material. In the present case, no segregation was detected by SEM or TEM-EDX spectroscopy in the main trunk or the branches of the structures, but incorporation of a small concentration of metallic elements (Sn and Er) below the EDX detection limit is certainly possible. In fact, previous works reported alloying metallic elements contents below 0.5 at% in certain areas of the hierarchical nanostructures while in others such elements were not detected.^{25,26}

The XRD spectra of all the grown samples were indexed to the monoclinic $\alpha\text{-Bi}_2\text{O}_3$ phase (JCPDS card 041-1449), regardless of the precursor used and the final morphology of the structures (Fig. 3). Moreover, no diffraction maxima related to pure Sn, Er or their corresponding oxides were observed. EDX spectra in SEM (Fig. 4) or TEM reveal only peaks corresponding to Bi and O and no Sn or Er signals were detected. For these reasons, the structures obtained from both kinds of precursors were considered to be equivalent regarding crystallography and composition. Since the presence of Er_2O_3 yielded thin nanowires and a higher density of branched structures, mainly the samples obtained from the precursor mixture Bi- Er_2O_3 were further investigated.

Individual nanowires with diameters of several hundreds of nanometres were selected for EBSD characterization in the SEM. EBSD allows crystallographic information to be obtained from samples in the SEM by striking an electron beam on a tilted sample and obtaining the diffracted electron pattern with the aid of a fluorescent phosphor screen. The variations of intensity of the diffracted electrons as a function of direction form patterns of Kikuchi lines. These diffraction patterns are then analyzed by computer software and used to measure the wire crystal orientation, discriminate between different materials and provide information about extended defects. EBSD was found to be particularly useful for the structural characterization of our Bi_2O_3 thicker structures, than cannot be properly

investigated by TEM. Such structures usually show smooth, well-faceted faces, where EBSD measurements can be carried out. A representative example of the acquired patterns is displayed in Fig. 5. The diffraction patterns did not change when the electron beam was moved along the length of the wire. The obtained results reveal that all the wires investigated are of monoclinic structure and belong to the α - Bi_2O_3 phase, usually with a [011] zone axis. Our EBSD studies did not reveal the presence of extended defects in these samples.

Low magnification TEM images of the secondary nanowires (those that stem from the central axis) show branched nanostructures with lengths up to 15 μm and diameters in the (40-300) nm range (Fig. 6a). A high-resolution micrograph of a 100 nm wide nanowire and the corresponding FFT pattern are shown in Fig. 6b. Indexing of the FFT pattern and analysis of this and other images confirm that the wires belong to the monoclinic α -phase, as it was already reported for Bi_2O_3 nanowires grown by a similar procedure.³¹ The mentioned image shows fringes running perpendicular to the edge of the nanowire. The fringe spacing measures 0.82 nm, which corresponds to the (010) interplanar spacing. This shows the single crystalline nature of the wire, that grows along the [010] direction. A TEM image of the junction between two perpendicular nanowires is shown in Fig. 7a. HRTEM images of these regions, as that shown in Fig. 7b, revealed that the branched Bi_2O_3 nanowires have single-crystal structures with clean backbone-to-branch junctions. No extended defects were found in our HRTEM observations of similar areas, which strongly suggest that growth mechanisms driven by screw dislocations³² or twins³³ may be ruled out.

3.2 Luminescence

The influence of the precursor on the luminescence of the nanowires has been investigated by PL excited by 325 nm laser light. Although no Sn or Er have been detected in the analysis of the nanowires, luminescence can provide information on possible indirect effects of the addition of their oxides on the final defect structure and, in the case of Er, on the

presence of traces of optically active ions. In fact, the addition of Al_2O_3 to a ZnS precursor used to grow ZnO structures with the same vapour - solid method used in this work, has been found to induce the formation of branched nanorod networks and cathodoluminescence (CL) spectral changes without apparent Al incorporation into the structures, as measured by EDX.²⁶ These studies demonstrated that nanorod networks fabricated with Al_2O_3 -containing precursor show an emission band, attributed to oxygen excess, not observed in material prepared without Al_2O_3 or other oxides. In the present work, we compare the PL of the nanowires with previously reported PL studies of Bi_2O_3 sintered ceramics³⁴ and nanostructures.^{13,35} Fig. 8 shows the PL spectra of the nanowires grown with SnO_2 or Er_2O_3 in the precursor and a representative spectrum of Bi_2O_3 ceramics prepared by sintering pure Bi_2O_3 powders at 500 °C for 10 h. The obtained results indicate that modifying the composition of the source materials changes not only the morphology of the grown oxide nanostructures, but also their luminescence properties. Actually, it can be observed that the three spectra have their maxima at different energies. The observed shifts cannot be attributed to quantum confinement effects or residual stresses within the Bi_2O_3 nanowires,¹³ since SEM images reveal nanostructures with dimensions above 100 nm while TEM observations provide no evidence of lattice distortions. As explained below, the different peak positions observed in PL spectra of nanowires grown by adding the mentioned two oxides are due to the relative weights of the different emission bands contributing to the overall spectrum in each case.

The spectrum of the ceramic sample is peaked at 2.33 eV (532 nm), but previous CL investigations reveal the existence of other components at about 1.91 eV and 2.83 eV.³⁴ The 2.33 eV and the 1.95 eV emission bands have been attributed to a Bi ion in a closest environment of three oxygen ions.³⁶ Actually, trivalent bismuth cations in inorganic compounds exhibit interesting luminescence properties related to its $6s^2$ configuration.^{37,38} Above 80 K, radiative transitions are mainly assigned to $^3\text{P}_1 \rightarrow ^1\text{S}_0$ transitions^{13,35,37} or charge

transfer transitions between oxygen ligands and Bi^{3+} ions,³⁸ giving rise to luminescence spectra peaked in the blue to green region under UV excitation. On the other hand, Bi^{2+} ions show PL emission in the range 2.10 - 1.95 eV under UV excitation. This luminescence has been attributed to ${}^2\text{P}_{3/2}(1) \rightarrow {}^2\text{P}_{1/2}$ transitions^{35,39,40} and it is extremely dependent on the local crystal field, which in turn depends on the symmetry and coordination of the surrounding oxygen atoms. Our luminescence studies of Bi_2O_3 bulk samples annealed in different atmospheres have shown that a 2.1 eV band is related to oxygen vacancies.³⁴ Fig. 8 shows that the PL bands of the nanowires synthesized with precursors containing SnO_2 and Er_2O_3 appear peaked at 2.12 eV (585 nm) and 1.92 eV (646 nm), respectively. This indicates that the presence of Sn in the precursor favours the growth of nanowires with a higher concentration of oxygen vacancies. The diffusion of Bi ions has been previously considered to predominate over the diffusion of oxygen ions during the growth of complex Bi_2O_3 architectures by thermal oxidation of Bi, which resulted in the formation of a high density of oxygen vacancies.⁴¹ In the case of samples grown from the Er-containing precursor, the site symmetry and oxygen coordination around the reduced Bi ions favours an intense PL signal related to Bi^{2+} intraionic transitions.

3.3 Young's modulus

The characterization of the mechanical properties of semiconductor nanowires and other elongated nanostructures is a subject of interest related to their applications in NEMS, micromechanical sensors and optomechanical coupling devices.⁴² The Young's modulus of elongated nanostructures of different materials has been determined by electric field induced mechanical resonance, nanoindentation and atomic force microscopy. For reviews on mechanical characterization of nanowires, see refs. 42 and 43. In-situ TEM measurements of mechanical resonance under an applied electric field has enabled to determine the Young's modulus of ZnO nanobelts,⁴⁴ BN nanotubes,⁴⁵ carbon nanotubes,⁴⁶ or GaN nanowires.⁴⁷

Similar in-situ SEM studies which would enable to investigate larger nanowires have been only occasionally reported.⁴⁸ Measurements by mechanical resonance techniques and AFM have shown in some cases a strong dependence of the Young's modulus of elongated nanostructures on their geometrical parameters, as diameter of nanotubes⁴³ and nanowires⁴⁸ or width to thickness ratio of nanobelts.⁴⁹ In order to study such potential effects in our nanowires, the Young's modulus has been determined for a total of fourteen wires with different lengths and cross-sectional dimensions. By applying an alternating potential at the electrodes in the arrangement shown in the schematic of Fig. 1, the nanowires are deflected by the electrostatic force, leading to oscillations with the potential frequency. By measuring in the SEM screen the oscillation amplitude as a function of the frequency, an amplitude peak appears at the resonance frequency of the nanowire. In the present case, the resulting first harmonic resonance frequencies vary from 2 to 17 kHz. From elasticity theory⁵⁰ this resonance frequency is

$$\nu_i = \frac{\beta_i^2}{2\pi L^2} \sqrt{\frac{EI}{\rho S}} \quad (1)$$

where β_i is a constant for the i -th harmonic, L the length, E the Young's modulus, I the second moment of inertia ($I = \pi r^4/4$ for a cylindrical wire), ρ the density (8.9 gr/cm³ for α -Bi₂O₃) and S the cross-sectional area. From equation (1), the Young's modulus is

$$E = \frac{\nu_i^2 4\pi^2 L^4 \rho S}{I \beta_i^4} \quad (2)$$

which, for the first harmonic ($\beta_1 = 1.875$) and a cylindrical wire, is

$$E = (\nu L^2 / 0.28r)^2 \rho \quad (3)$$

where r is the radius of the nanowire.

Figs. 9a and 9b respectively show SEM images of a 250 μm long wire of 1 μm radius at rest and vibrating under the applied electric field. The amplitude-frequency curve of a wire of 500 nm radius is shown in Fig. 10a. The resonance frequency measurements in fourteen wires of different radii and lengths yielded a noticeable dispersion of E values, which ranged from 11 to 284 GPa. The relationship of the Young's modulus with the radius of the wires has been plotted in Fig. 10b. A general trend of a lower Young's modulus for higher radius can be appreciated. Such trend is qualitatively similar to that reported for ZnO,⁴⁸ CuO,⁵¹ WO₃,^{52,53} Ag and Pb nanowires,⁵⁴ but in the present case the effect is observed for larger radii. In some works, the measured values of E approach the bulk value as the radius of the nanowire increases.^{47,48,51} This size dependence has been explained for ZnO nanowires in terms of surface stiffening arising from the gradually shortened bond lengths from the nanostructure central region to the surface.⁴⁸ A similar trend has also been reported for CuO nanowires and attributed to the formation of an amorphous layer in the smaller nanostructures.⁵¹ However, in other cases the opposite trend has been observed, i.e., the Young's modulus approaches the bulk value as the radii of the nanowires decrease.^{52,53} This has been explained by differences in the defect structure of nanowires with different diameters. Since we are not aware of previous works reporting the Young's modulus of α -Bi₂O₃, a bulk ceramic sample of this oxide was prepared by sintering pure Bi₂O₃ powder at 750 °C for 10 h. The ceramic was mirror polished and the corresponding Young's modulus determined by nanoindentation.⁵⁵ The obtained value, (105 \pm 4) GPa, is included in

the interval shown in Fig. 10a and also in good agreement with the 104 GPa value that can be deduced from the elastic constants calculated by Music et al.⁵⁶ for bulk δ - Bi_2O_3 . These results suggest that surface effects do not play a dominant role in the observed trend of E as a function of the wire radius.

The quality factor Q of the microwires as mechanical resonators can be estimated from fitting of the resonance curves to Lorentzian profiles, as expected for damped harmonic vibrations, according to the relationship $Q = \nu_r/\Delta\nu$, where ν_r is the peak resonance frequency and $\Delta\nu$ is the full-width at half-maximum of the resonance peak. The inverse factor $1/Q$ is related to the energy dissipation. Since the wires vibrate at SEM vacuum ($\sim 10^{-6}$ Torr), the energy dissipation arising from air damping can be neglected; it mainly originates from the intrinsic properties of the material. Measurements of Q in the obtained resonance curves yield values in the range 650 - 750. Reported quality factors for mechanical resonances of semiconducting nanowires or nanotubes extend over a wide range of values, which are in many cases comparable to those measured in this work, *e.g.*, 120 for V_2O_5 nanowires,⁵⁷ 20-750 for SiO_2 nanowires,⁵⁸ 340 for boron nitride nanotubes,⁴⁵ 500 for ZnO nanobelts⁴⁴ or 80-700 for MoS_2 diaphragms.⁵⁹ These results show that Bi_2O_3 wires may have potential application as micromechanical resonators.

4. Conclusions

Hierarchical Bi_2O_3 nano- and microwires grown by a thermal evaporation-deposition method have been investigated. The addition of SnO_2 or Er_2O_3 to the

main Bi precursor favours the formation of hierarchical, multi-branched, arrangements. The incorporation of Er or Sn to Bi_2O_3 nanostructures was not detected by SEM or TEM-EDX microanalysis, but both metallic elements may be present in concentrations below the detection limit of this analytical technique. XRD, EBSD and HRTEM measurements reveal the good crystallinity of the grown samples, the structure of which corresponds to the monoclinic $\alpha\text{-Bi}_2\text{O}_3$ phase. The composition of the precursors influences not only the morphology but also the luminescence properties of the oxide nanostructures. PL of the nanowires shows that the relative intensities of emission bands associated to Bi^{2+} ions and to oxygen vacancies depend on the composition of the precursor used to grow the nanostructures. In-situ SEM mechanical resonance induced by an alternating electric field has been used to determine the Young's modulus of the microwires. A noticeable dispersion of E values has been obtained with a trend toward smaller values for increasing radius of the microwires. The quality factors measured for the microstructures suggest that Bi_2O_3 wires may have potential application as micromechanical resonators.

Acknowledgements

This work has been supported by MINECO through projects CSD2009-00013, MAT 2012-31959 and MAT 2010-16407.

References

- 1 Y. Cui and C. M. Lieber, *Science*, 2001, **291** 851-853.
- 2 M. Willander, L. L. Yang, A. Wadeasa, S. U. Ali, M. H. Asif, Q. X. Zhao and O. Nura, *J. Mater. Chem.*, 2009, **19**, 1006-1018.
- 3 Guoqing Wang, Hirofumi Tanaka, Liu Hong, Yasutaka Matsuo, Kenichi Niikura, Masuhiro Abe, Kazuhiko Matsumoto, Takuji Ogawab and Kuniharu Ijira, *J. Mater. Chem.*, 2012, **22**, 13691-13697.
- 4 Zhong Lin Wang, *J. Phys.: Condens. Matter*, 2004, **16**, R829–R858.
- 5 Chao Li, Daihua Zhang, Xiaolei Liu, Song Han, Tao Tang, Jie Han and Chongwu Zhou, *Appl. Phys. Lett.*, 2003, **82**, 1613-1615.
- 6 Liang Cheng, Ming-Wang Shao, Dayan Chen, Dorothy Duo Duo Ma and Shuit-Tong Lee, *CrystEngComm*, 2010, **12**, 1536-1539.
- 7 H. Gobrecht, S. Seeck, H. E. Bergt, A. Märten and K. Kossmann, *Phys. Stat. Sol.* 1969, **33**, 599-606.
- 8 M. Vila, C. Díaz-Guerra and J. Piqueras, *J. Alloys Compd.* 2013, **548**, 188-193.
- 9 Cabot, A. Marsal, J. Arbiol and J.R. Morante, *Sens. Actuators B*, 2004, **99**, 74-89.
- 10 A. Hameed, T. Montini, V. Gombac and P. Fornasiero, *J. Am. Chem. Soc.*, 2008, **130**, 9658-9659.
- 11 L. Leontie, M. Caraman, M. Alexe and C. Harnagea, *Surf. Sci.*, 2002, **480**, 507-510.
- 12 M. Vila, C. Díaz-Guerra and J. Piqueras, *J. Mater. Chem. C*, 2013 **1**, 7920-7929.
- 13 Latha Kumari, Jin-Han Lin and Yuan-Ron Ma, *J. Phys: Condens. Matter*, 2007, **19**, 406204.
- 14 Yongfu Qiu, Minlin Yang, Hongbo Fan, Yuanzhi Zuo, Youyuan Shao, Yongjun Xu, Xiaoxi Yanga and Shihe Yang, *CrystEngComm*, 2011, **13**, 1843–1850.
- 15 H. W. Kim, J. W. Lee and C. Lee, *J. Korean. Phys. Soc.*, 2007, **50**, 1308-1311.

- 16 X.P. Shen, S.K. Wu, H. Zhao and Q. Liu, *Physica E*, 2007, **39**, 133-136.
- 176 S. Park, H. Kim, C. Lee, D.H. Lee and S.S. Hong, *J. Korean Phys. Soc.*, 2008, **53**, 1965-1970.
- 18 X. Gou, R. Li, G. Wang, Z. Chen and D. Wexler, *Nanotechnology*, 2009, **20**, 495501.
- 19 B. Ling, X. W. Sun, J. L. Zhao, Y. Q. Shen, Z. L. Dong, L. D. Sun, S. F. Li and S. Zhang, *J. Nanosci. Nanotechnol.* 2010, **10**, 8322-8327.
- 20 Di Chen, Zhe Liu, Xianfu Wang, Bo Liang, Jing Xu, Hongtao Huang, Zhong Xie and Guozhen Shen, *CrystEngComm*, 2011, **13**, 7305-7310.
- 21 Jing Yu Lao, Jian Guo Wen and Zhi Feng Ren, *Nano Lett.* 2002, **2**, 1287-1291.
- 22 J. G. Wen, J. Y. Lao, D. Z. Wang, T. M. Kyaw, Y. L. Foo, Z. F. Ren, *Chem. Phys. Lett.*, 2003, **372**, 717-722.
- 23 Puxian Gao and Zhong Lin Wang, *J. Phys. Chem. B*, 2002, **106**, 12653-12658.
- 24 Y. Ortega, P. Fernández and J. Piqueras, *J. Cryst. Growth*, 2009, **311**, 3231-3234.
- 25 Y. Ortega, P. Fernández and J. Piqueras, *J. Nanosci. Nanotechnol.*, 2010, **10**, 502-507.
- 26 Y. Ortega, P. Fernández and J. Piqueras, *Semicond. Sci. Technol.*, 2011, **26**, 085035.
- 27 P. Hidalgo, B. Méndez and J. Piqueras, *Nanotechnology*, 2008, **19**, 455705.
- 28 I. López, E. Nogales, B. Méndez, J. Piqueras, A. Peche, J. Ramírez-Castellanos and J. M. González – Calbet, *J. Phys. Chem. C*, 2013, **117**, 3036-3045.
- 29 Zu Rong Zai, Zheng Wei Pan and Zhong L. Wang, *Adv. Funct. Mater.* 2003, **13**, 9-24.
- 30 Samuel L. Mensah, Abhishek Prasad, Jiesheng Wang and Yoke Khin Yap, *J. Nanosci. Nanotechnol.* 2008, **8**, 233-236.
- 31 M. Vila, C. Díaz-Guerra and J. Piqueras, *Appl. Phys. Lett.*, 2012, **101**, 071905.
- 32 Jia Zhu, Hailin Peng, A. F. Marshall, D. M. Barnett, W. D. Nix and Yi Cui, *Nature Nanotechnology*, 2008, **3**, 477-481.

- 33 Dongsheng Li, Frank Soberanis, Jia Fu, Wenting Hou, Jianzhong Wu and David Kisailus, *Cryst. Growth Des.*, 2013, **13**, 422-428.
- 34 M. Vila, C. Díaz-Guerra and J. Piqueras, *Mater. Chem. Phys.*, 2012, **133**, 559-564.
- 35 Latha Kumari, Jin-Han Lin and Yuan-Ron Ma, *Nanotechnology*, 2007, **18**, 295605.
- 36 O. M. Bordun, I. I. Kukhasrskii, V. V. Dmitruk, V. G. Antonyuk and V. P. Savchin, *J. Appl. Spectrosc.*, 2008, **75**, 681-684.
- 37 G. Blasse, H. Zhiran, A.J.A. Winnubst and A.J. Burggraaf, *Mat. Res. Bull.*, 1984 **19**, 1057-1062.
- 38 Y. Zorenko, V. Gorbenko, T. Voznyak, V. Jary and M. Nikl, *J. Lumin.*, 2010, **130**, 1963-1969.
- 39 A. M. Srivastava, *J. Lumin.*, 1998, **78**, 239-243.
- 40 M. Gaft, R. Reisfeld, G. Panczer, G. Boulon, T. Saraidarov and S. Erlich, *Opt. Mater.*, 2001, **16**, 279-290.
- 41 Xiangyang Liu, Weiguo Bian and Changyan Tian, *Mater. Lett.* 2013, **112**, 1-4.
- 42 C. Röhling, M. Niebelschütz, K. Brueckner, K. Tonisch, O. Ambacher and V. Cimalla, *Phys. Status Solidi B*, 2010, **247**, 2557-2570.
- 43 Z. L. Wang, *Dekker Encyclopedia of Nanoscience and Nanotechnology*, Eds. J.A. Schwarz, C. Contescu and K. Putyera, Marcel Dekker, Inc. 2004, 1773-1786.
- 44 X. D. Bai, P. X. Gao, Z. L. Wang and E. G. Wang, *Appl. Phys. Lett.*, 2003, **82**, 4806-4808.
- 45 A. P. Suryavanshi, M. Yu, J. Wen, C. Tang and Y. Bando, *Appl. Phys. Lett.*, 2004, **84**, 2527-2529.
- 46 P. Poncharal, Z. L. Wang, D. Ugarte and W. A. de Heer, *Science*, 1999, **283**, 1513-1516.
- 47 Chang-Yong Nam, Papot Jaroenapibal, Douglas Tham, David E. Luzzi, Stephane Evoy, and John E. Fischer, *Nano Lett.*, 2006, **6**, 153-158.
- 48 C. Q. Chen, Y. Shi, Y. S. Zhang, J. Zhu and Y. J. Yan, *Phys. Rev. Lett.*, 2006, **96**, 075505.

- 49 M. Lucas, W. Mai, R. Yang, Z. L. Wang and E. Riedo, *Nano Lett.*, 2007, **7**, 1314-1317.
- 50 W. Weaver, S. P. Timoshenko and D. H. Young, *Vibration Problems in Engineering*, 5th edition, 1990, John Wiley & Sons Inc., New York.
- 51 E. P. S. Tan, Y. Zhu, T. Yu, L. Dai, C. H. Sow, V. B. C. Tan and C. T. Lin, *Appl. Phys. Lett.*, 2007, **90**, 163112.
- 52 K. H. Liu, W. L. Wang, Z. Xu, L. Liao, X. D. Bai and E. G. Wang, *Appl. Phys. Lett.*, 2006, **89**, 221908.
- 53 Fook Chiong Cheong, Binni Varghese, Yanwu Zhu, Eunice Phay Shing Tan, Ling Dai, Vincent B. C. Tan, Chwee Teck Lim and Chorng Haur Sow, *J. Phys. Chem. C*, 2007, **111**, 17193-17199.
- 54 Stéphane Cuenot, Christian Frétigny, Sophie Demoustier-Champagne and Bernard Nysten, *Phys. Rev B*, 2004, **69**, 165410.
- 55 Jon Molina, private communication, jon.molina@imdea.org.
- 56 Denis Music, Stephanos Konstantinidis and Jochen M. Schneider, *J. Phys.: Condens. Matter*, 2009, **21**, 175403.
- 57 Yanwu Zhu, Yousheng Zhang, Ling Dai, Fook-Chiong Cheong, Vincent Tan, Chorng-Haur Sow and Chwee-Teck Lim, *Acta Mater.*, 2010, **58**, 415-420.
- 58 D. A. Dikin, X. Chen, W. Ding, G. Wagner and R. S. Ruoff, *J. Appl. Phys.*, 2003, **93**, 226-230.
- 59 Jaesung Lee, Zenghui Wang, Keliang He, Jie Shan and Philip X.-L. Feng, *ACS Nano*, 2013, **7**, 6086-6091.

Figure Captions

Fig. 1. Experimental setup used for in-situ mechanical resonance measurements in the SEM.

Fig. 2. (a) SEM image of a hierarchical structure grown from the precursor containing SnO₂. (b) SEM image of the same structure showing branched secondary parallel rods. SEM images (c) and (d) show hierarchical structures obtained after thermal treatment of the precursor with Er₂O₃, while figure (e) shows a wool-like arrangement of nanowires obtained by using the same precursor.

Fig. 3. XRD pattern representative of the hierarchical structures. All the diffraction maxima can be indexed to the monoclinic α -Bi₂O₃ phase (JCPDS card 041-1449).

Fig. 4. SEM-EDX spectrum of Bi₂O₃ nanowires grown from the precursor containing Er₂O₃. Only peaks related to O and Bi can be appreciated.

Fig. 5. Indexed EBSD pattern of a 500 nm wide Bi₂O₃ wire with the symmetries of the monoclinic α phase.

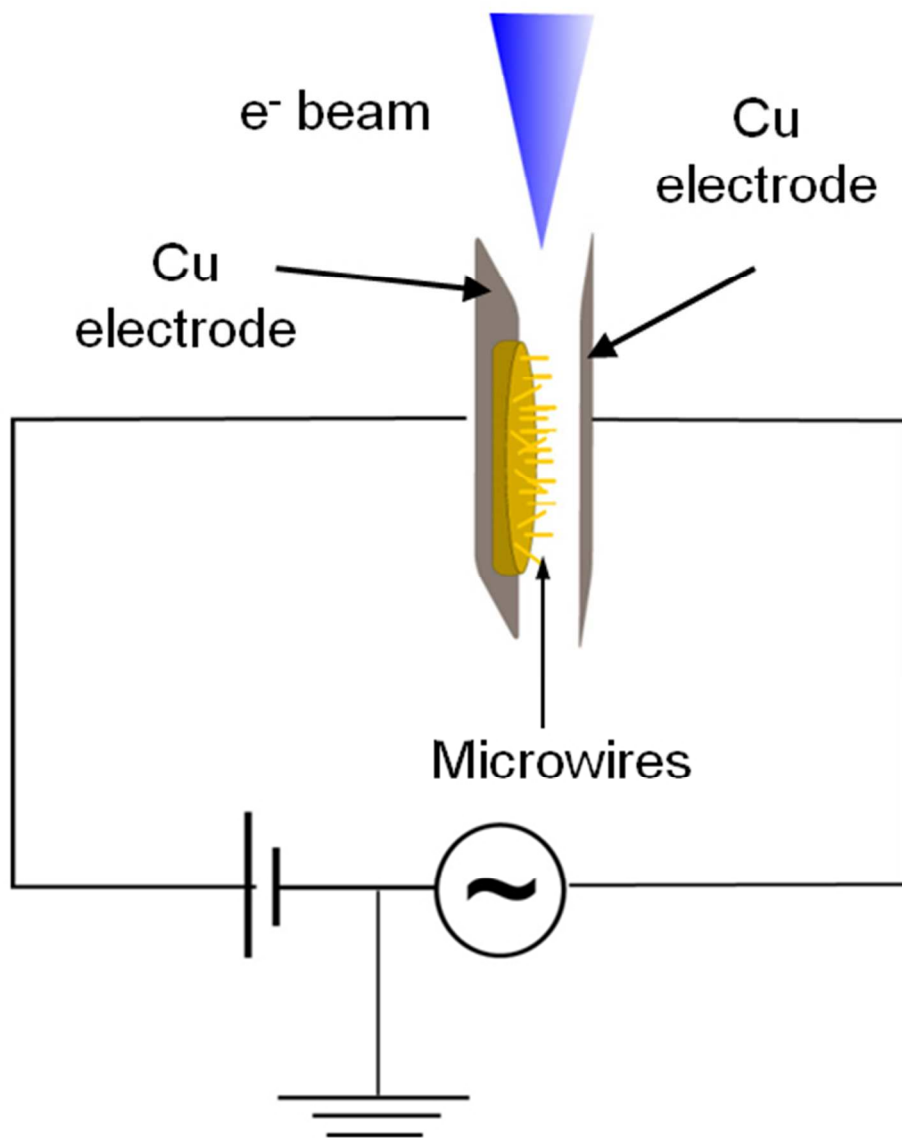
Fig. 6. Low magnification TEM image showing a group of branched nanowires (a). HRTEM image of a 100 nm wide nanowire showing the (010) interplanar distance of α -Bi₂O₃. The inset shows the corresponding indexed FFT pattern.

Fig. 7. (a) TEM micrograph of the junction between two perpendicular nanowires. (b) HRTEM image of the same area showing single-crystal structures with no extended defects.

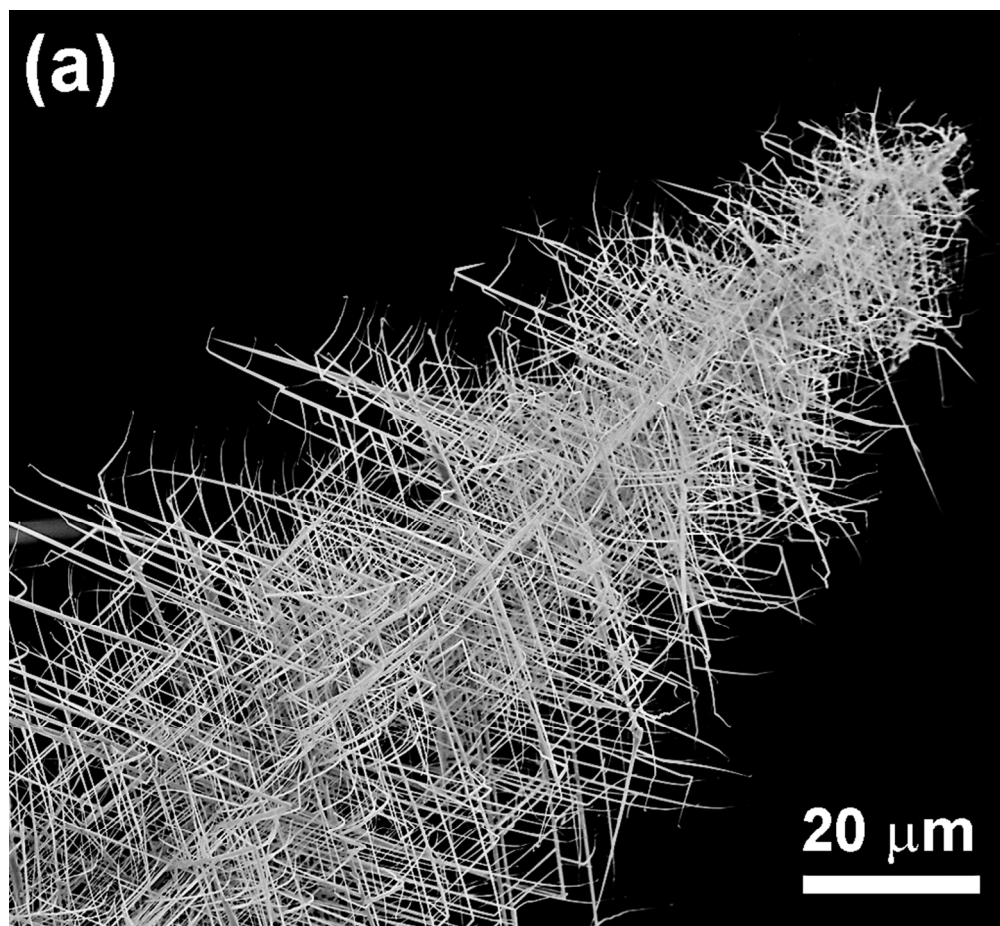
Fig. 8. PL spectra of α -Bi₂O₃ nanowires grown from different precursors and of a bulk ceramic sample sintered for comparison purposes.

Fig. 9. SEM images of an α -Bi₂O₃ nanowire at rest (a) and vibrating under the applied alternating electric field (b).

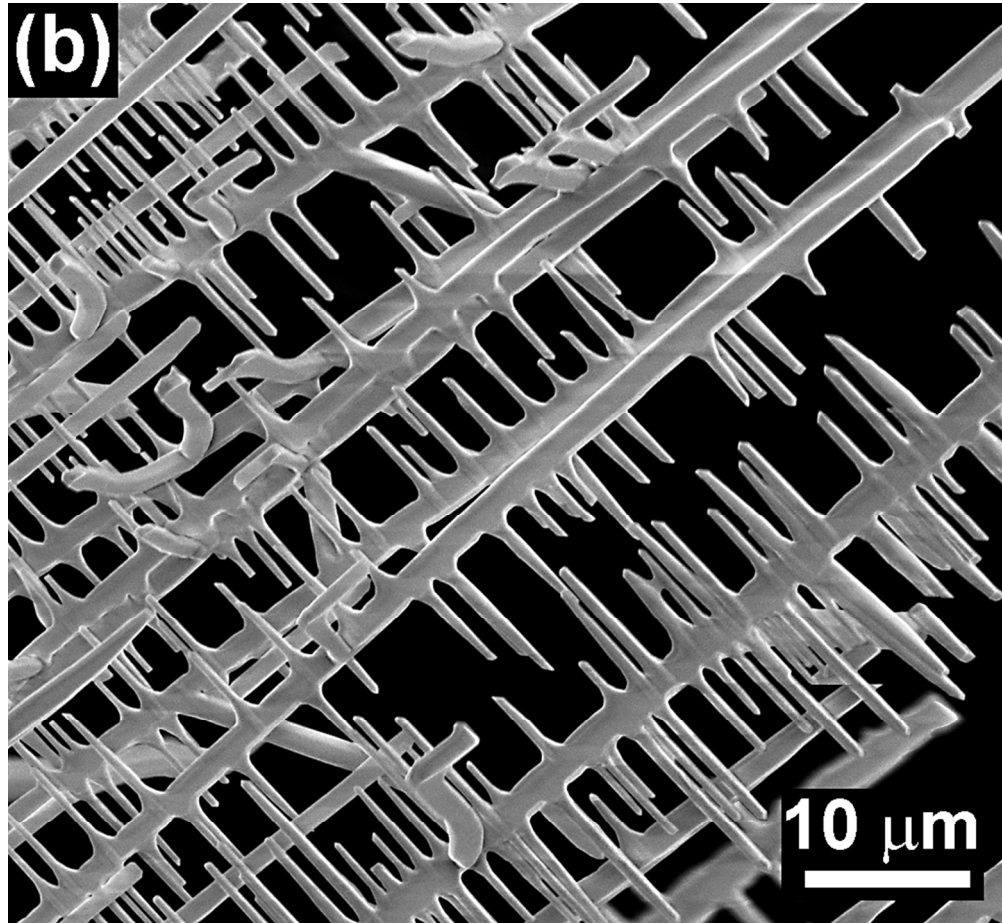
Fig. 10. (a) Response curve for the resonance of a Bi₂O₃ microwire. The solid line is a Lorentzian fit for the experimental data, from which the Q factor is estimated to be 740. (b) Young's modulus of the microwires plotted as a function of its radii.



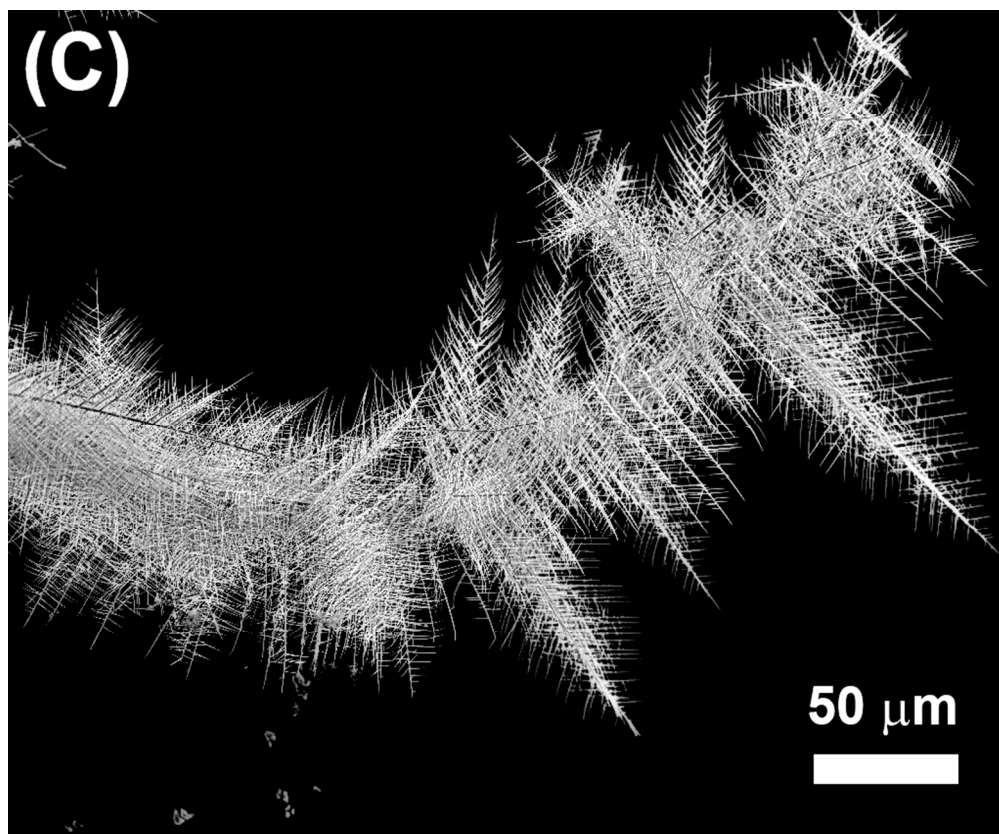
139x169mm (96 x 96 DPI)

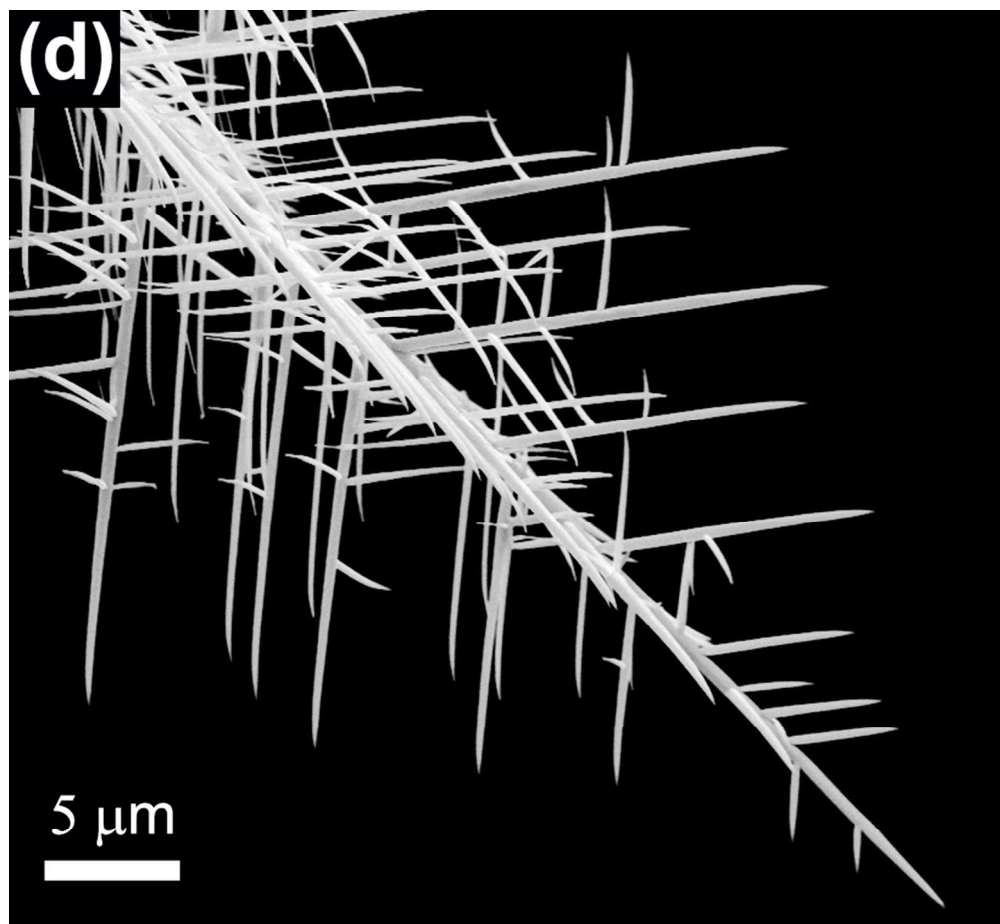


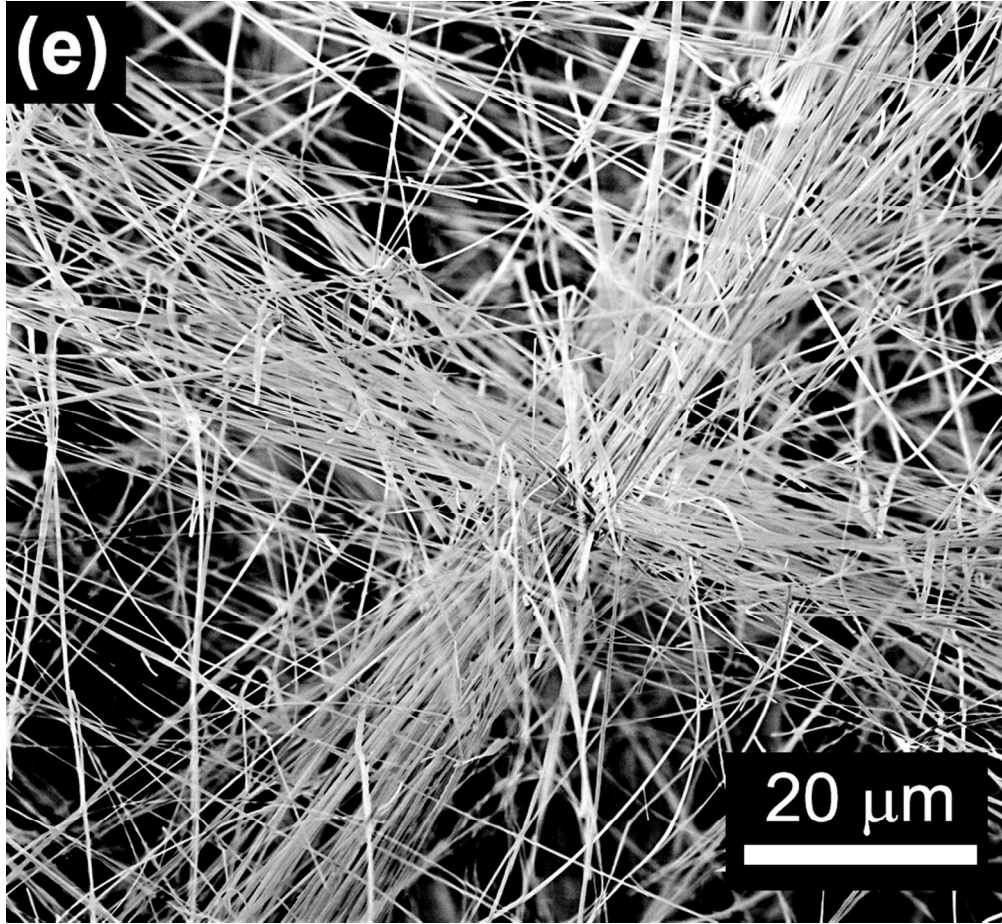
361x332mm (72 x 72 DPI)

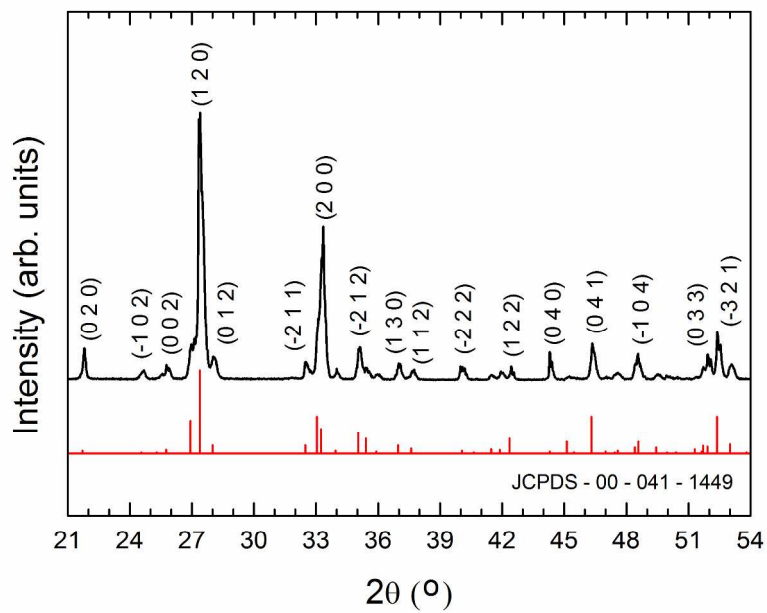


361x332mm (72 x 72 DPI)

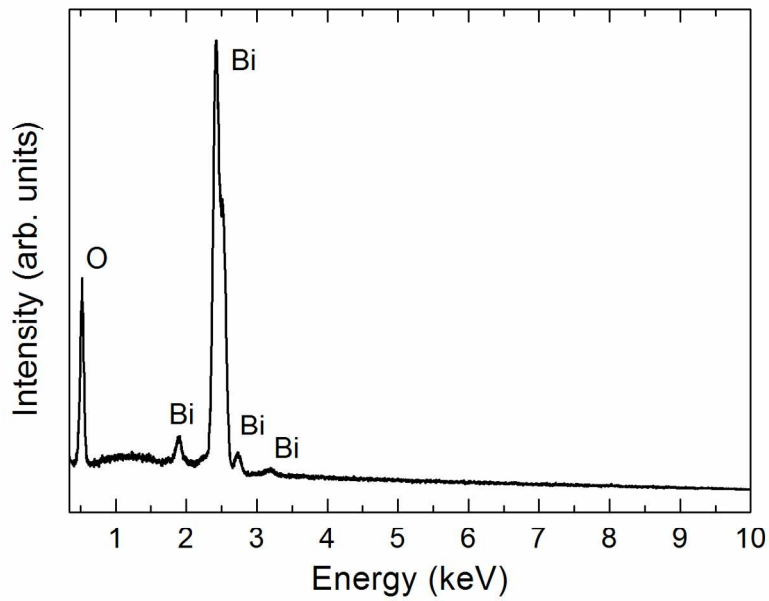




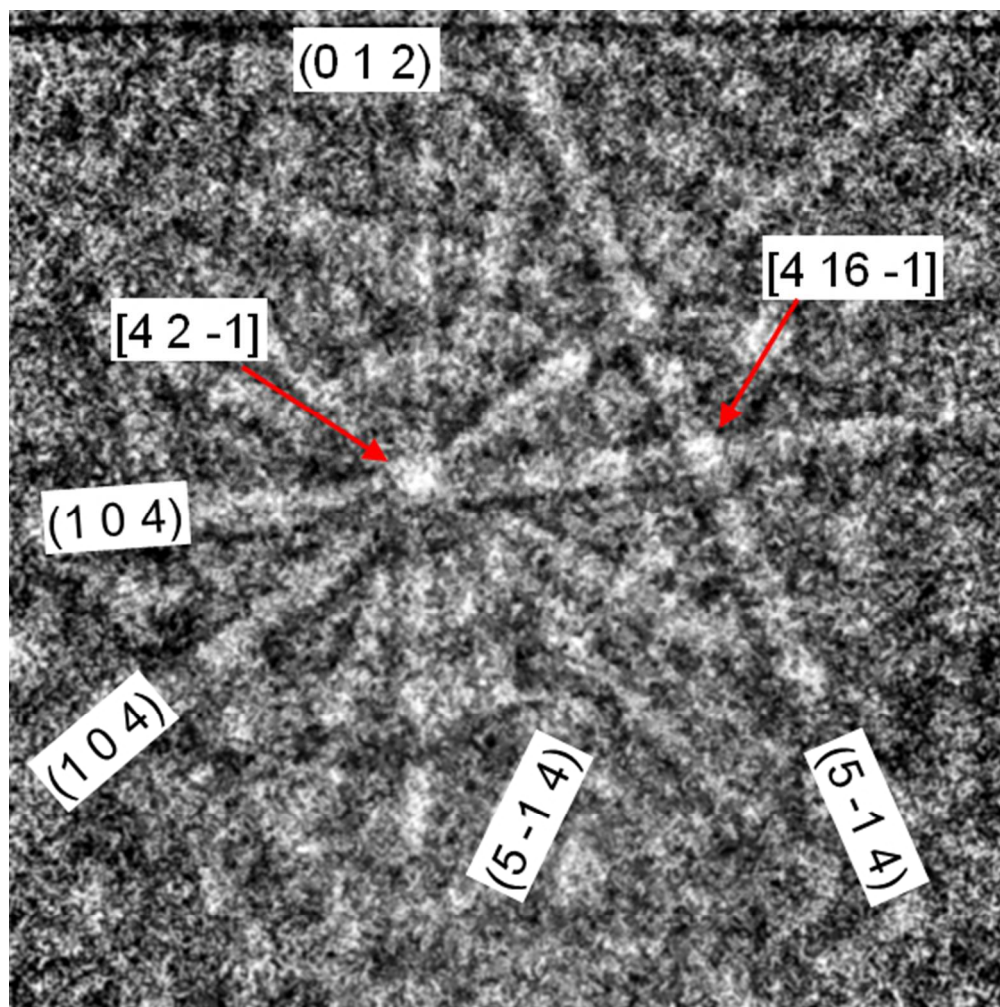




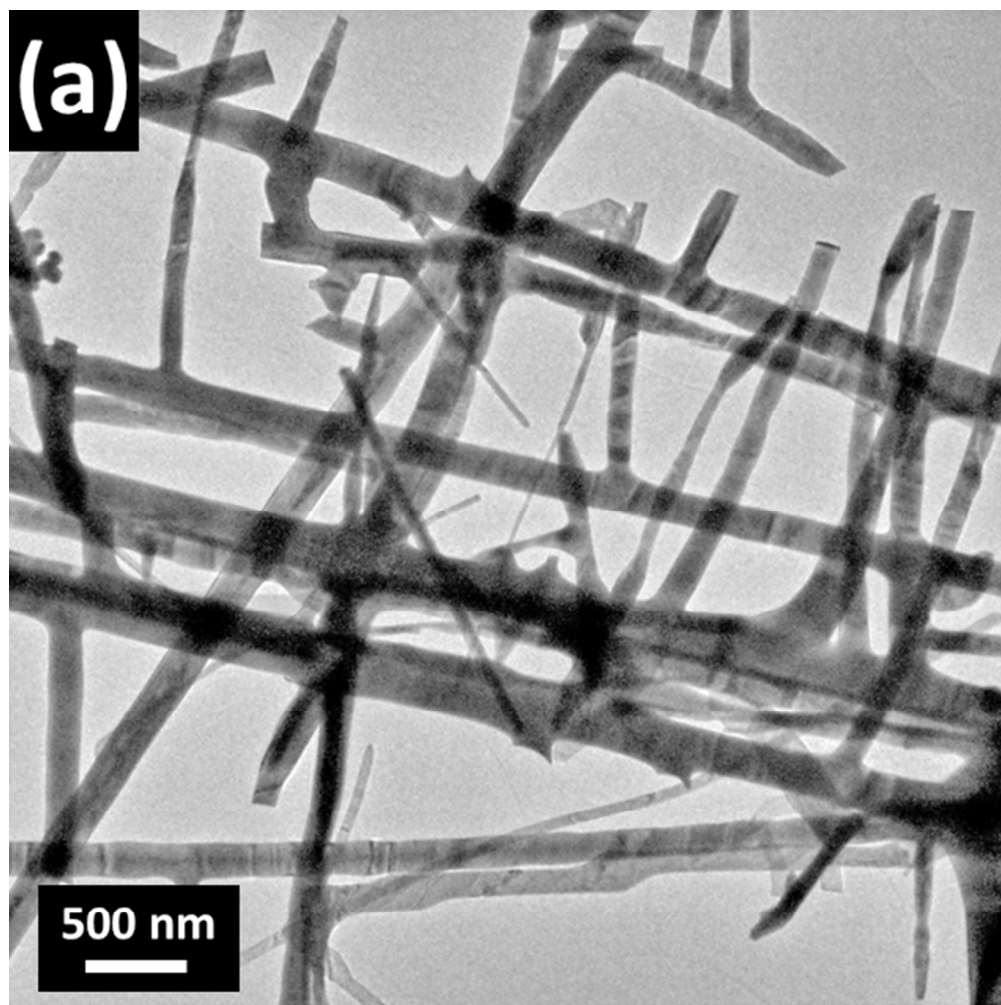
287x201mm (300 x 300 DPI)



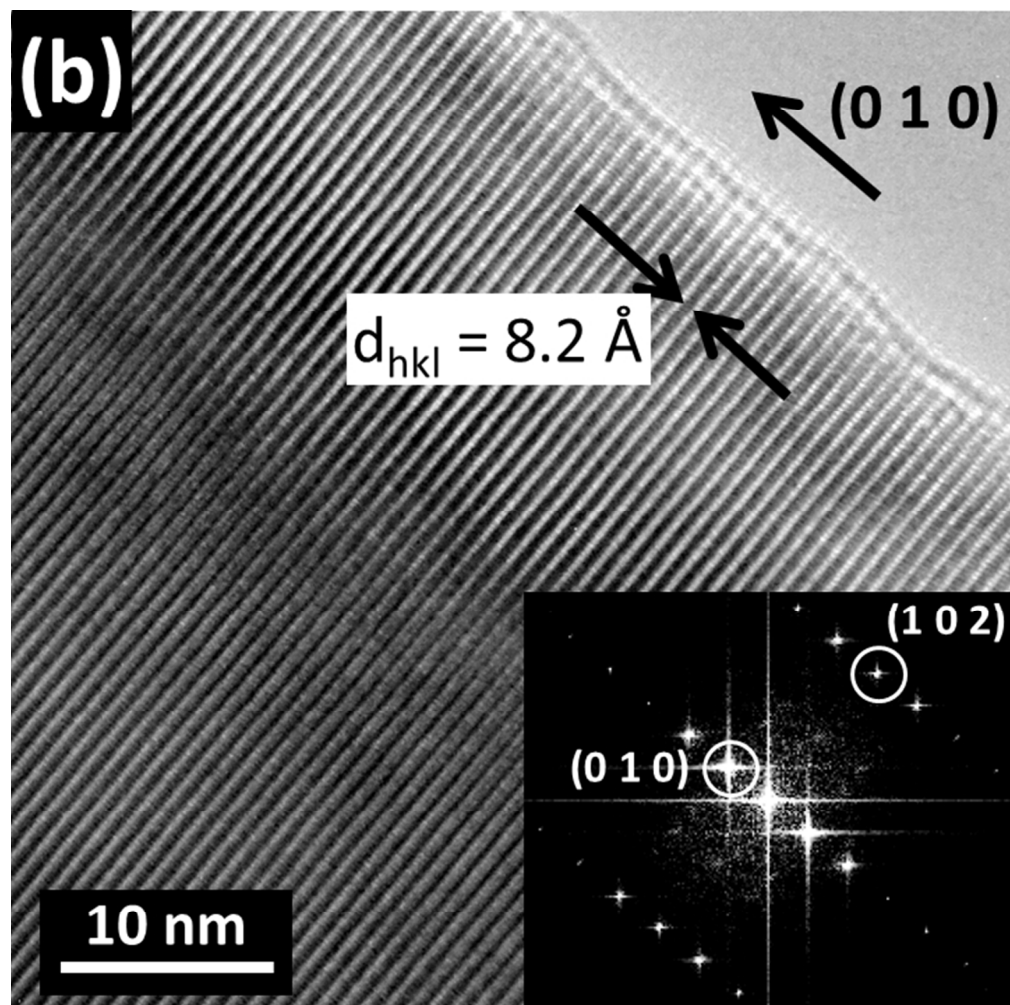
287x201mm (150 x 150 DPI)



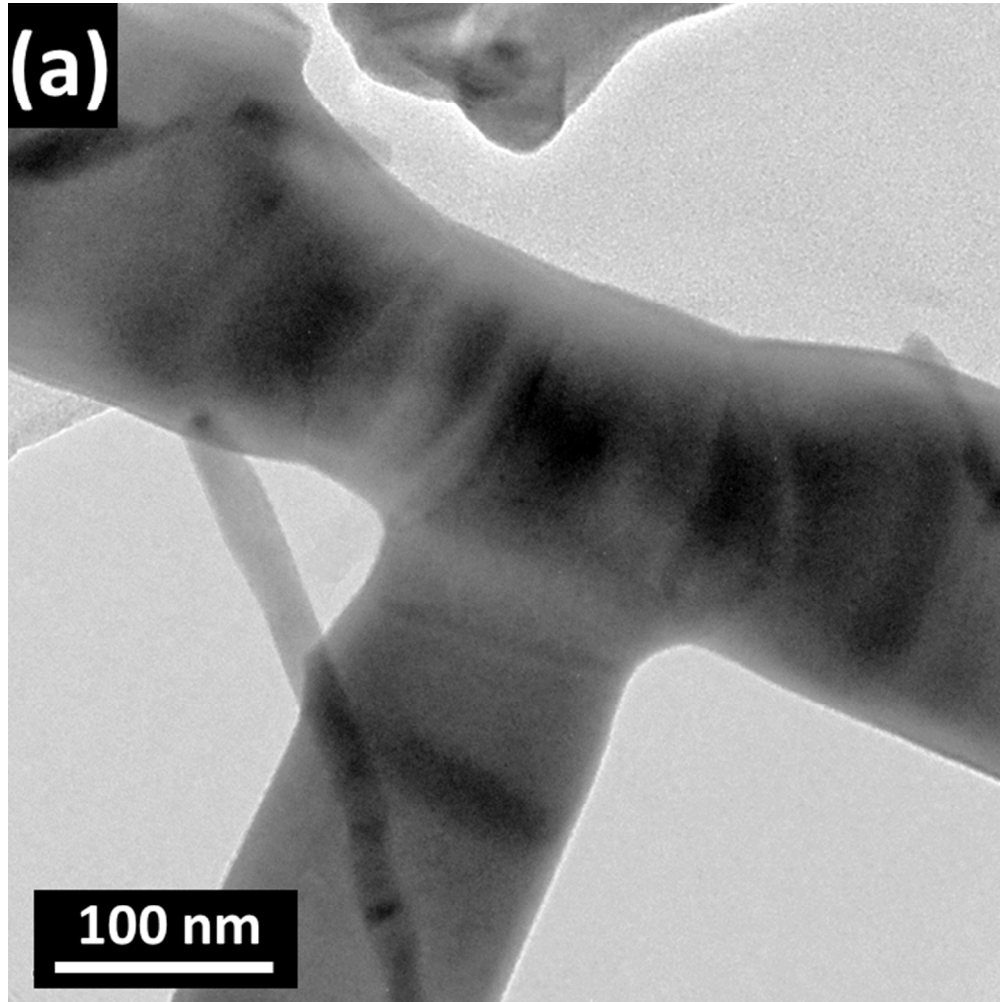
162x163mm (96 x 96 DPI)



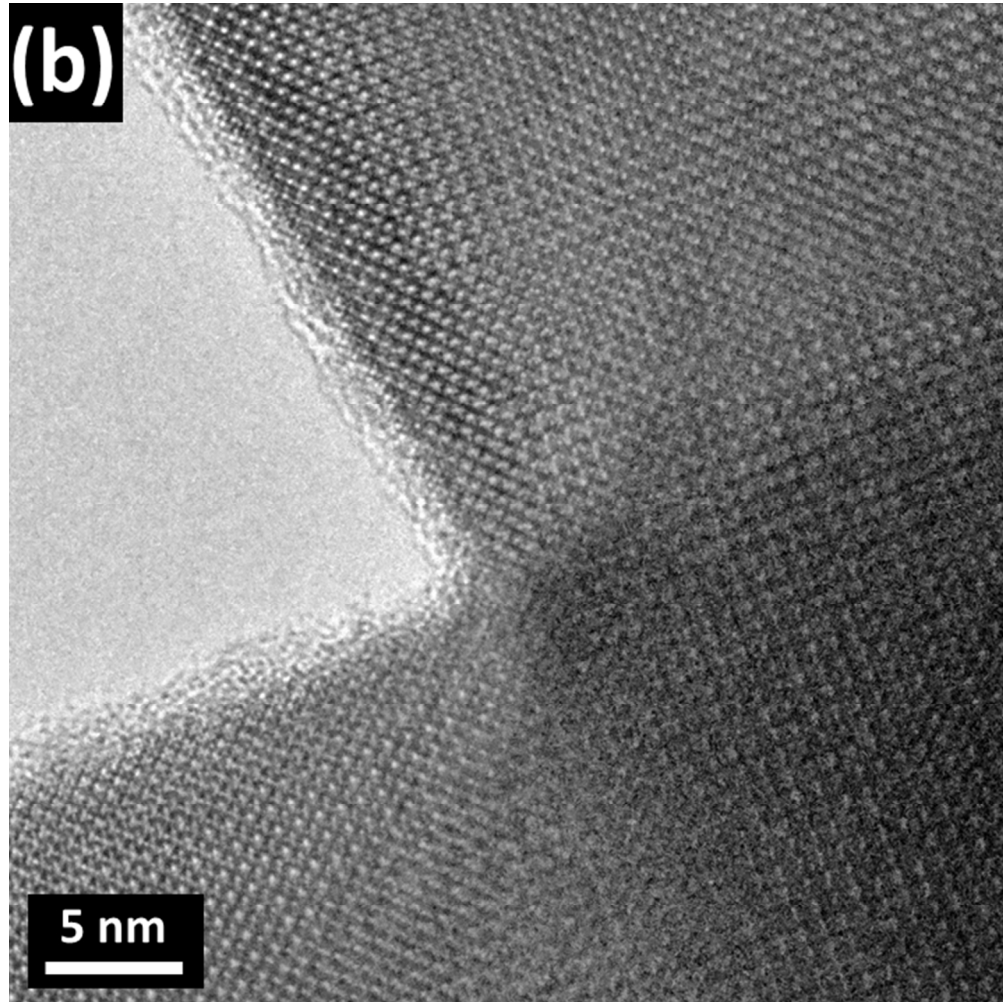
53x53mm (300 x 300 DPI)



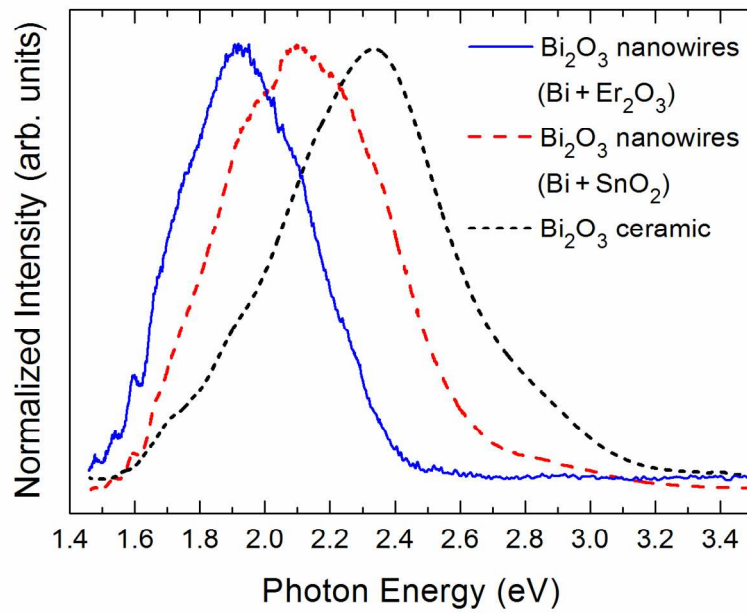
60x60mm (300 x 300 DPI)



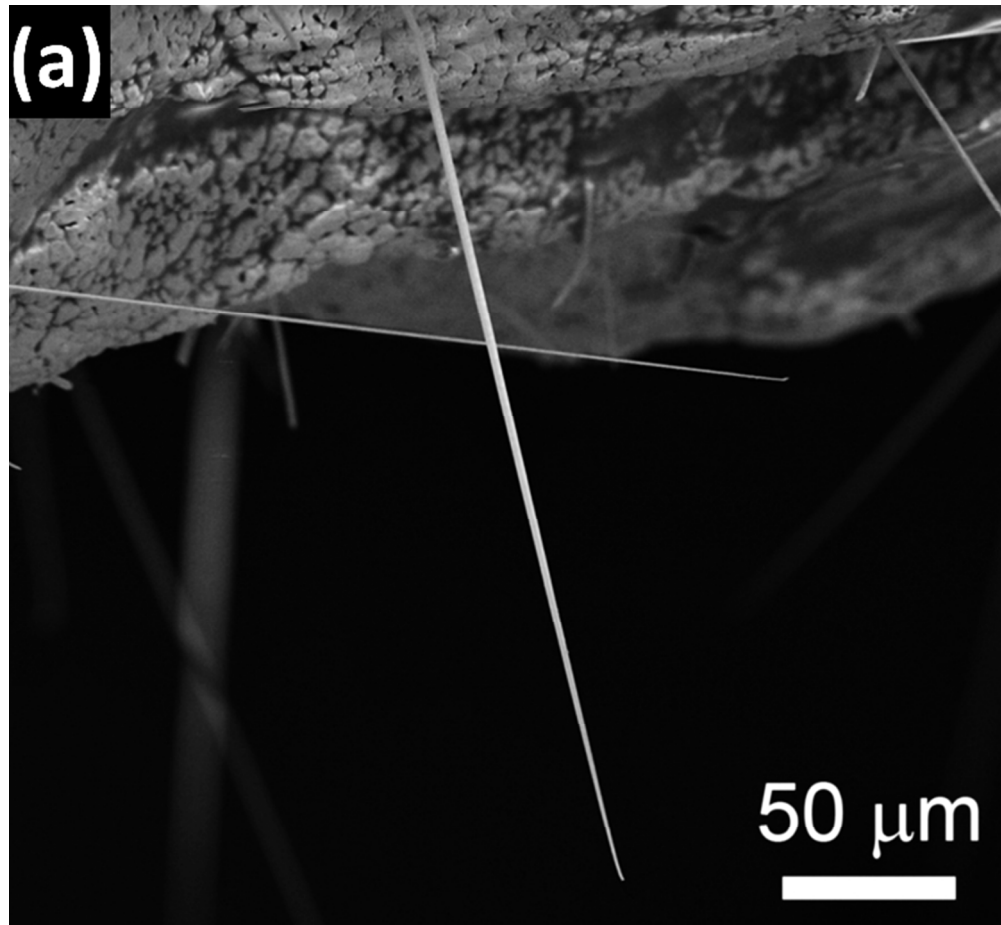
60x60mm (300 x 300 DPI)



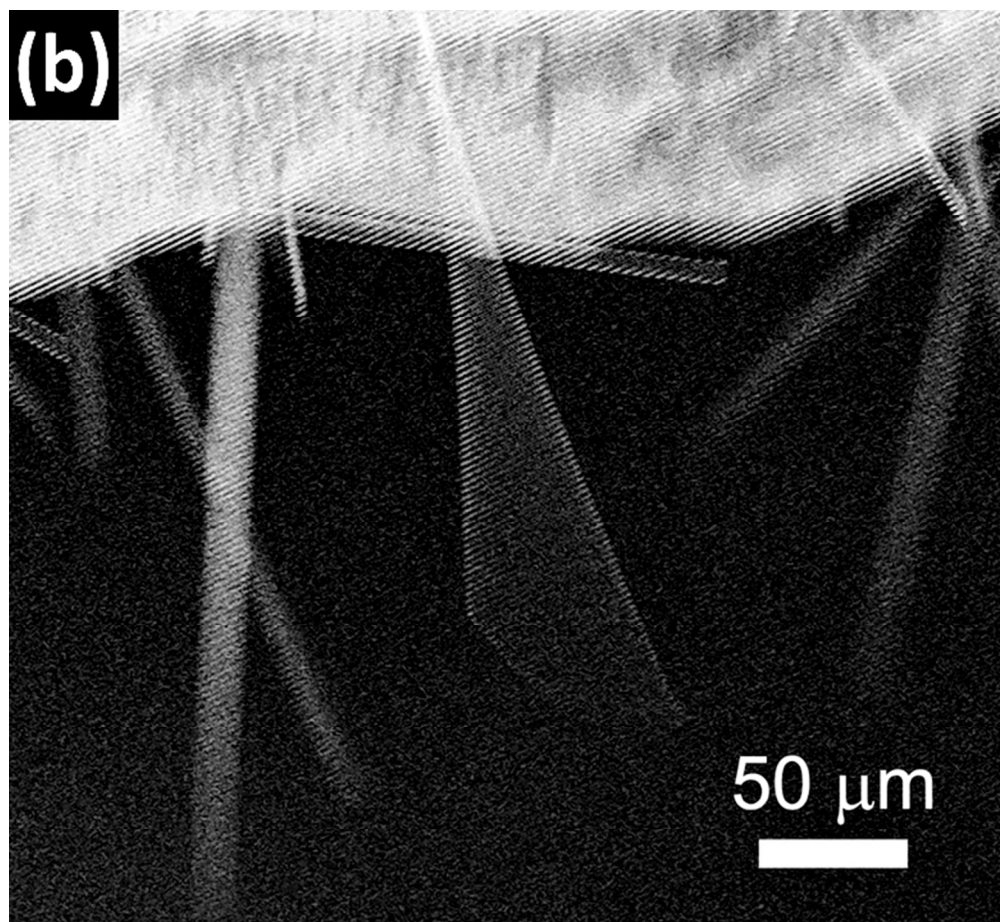
60x60mm (300 x 300 DPI)



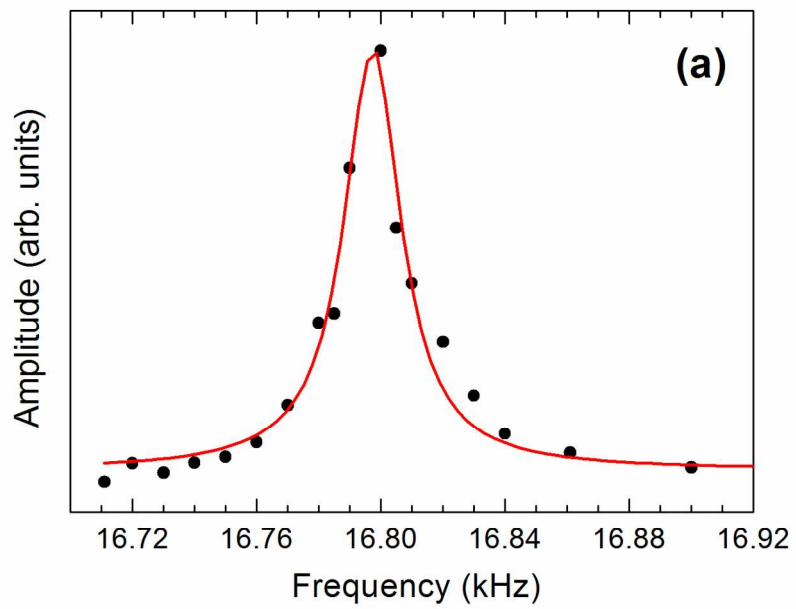
287x201mm (150 x 150 DPI)



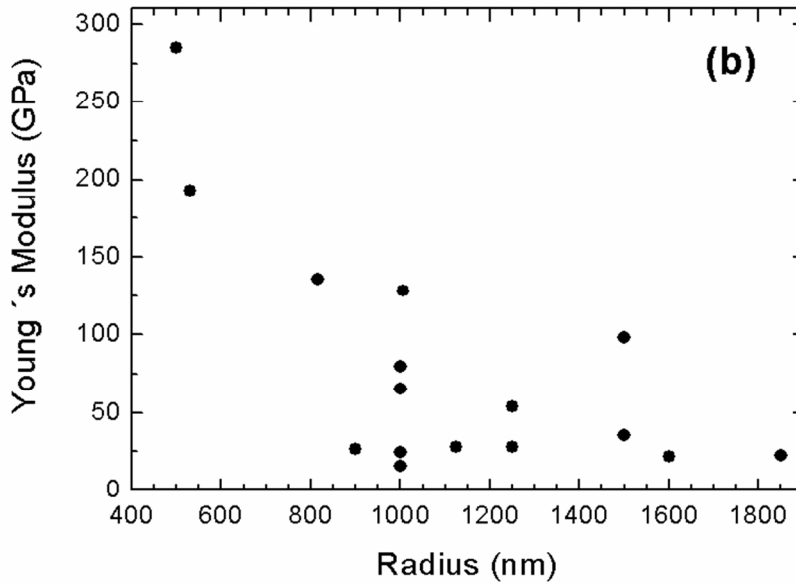
65x60mm (300 x 300 DPI)



66x60mm (300 x 300 DPI)



289x202mm (150 x 150 DPI)



79x61mm (300 x 300 DPI)